International Journal of Multiphase Flow, Vol. 94, September 2017, pp. 17-30
DOI:10.1016/j.ijmultiphaseflow.2017.04.007

An Inertial two-phase model of wax transport in a pipeline during pigging operations ⋆

Andrea Boghi[a,*], Lloyd Brown[b], Robert Sawko[c], Christopher P. Thompson[c]

[a]*School of Water, Energy and Environment, Cranfield University, Cranfield, Bedfordshire MK43 0AL, UK*
[b]*Science Deployed, LLC, Katy, Texas, United States*
[c]*AMAC Group, Cranfield University, Cranfield, Bedfordshire MK43 0AL, UK*

Abstract

Pig in pipelines performs operations for cleaning the pipe interior and internal inspection. In the past few years many 1D models have been developed to simulate the process because of their reduced computational cost; however, they rely on simplifications which are not always valid. In this paper, the results of a three-dimensional (3D) numerical investigation of the interaction between a waxy-oil and a dynamic sealing pig in a pipeline are presented. The results are obtained at a reduced computational cost by using a moving frame of reference, and an "injection" boundary condition for the wax deposited on the wall. The effect of the temperature and the wax particles' size has been investigated. The 3D results show the structure assumed by the debris field in front of the pig. In particular, a lubrication region at the bottom of the pipe, whose dimensions are temperature dependent, is shown. This information cannot be deduced from 1D modeling. The influence of the oil on the mixture viscosity and the internal bed dynamics are discussed. This work provides insights into the interaction between the debris field in front of the pig and pipeline hydraulics.

Keywords: pigging, oil, wax, deposition, pipeline, modeling

⋆Modeling wax transport during pigging operations

*A. Boghi
Email address: a.boghi@cranfield.ac.uk (Andrea Boghi)
[1]A. Boghi
[2]L. Brown
[3]R. Sawko
[4]C. P. Thompson

1. Introduction

Pipelines are the most common and safest way to transport oil and gas products. During operation, the pipeline walls suffer a deterioration process and can fail if they are not properly maintained. One part of pipelines maintenance procedure is "pigging" them regularly to prevent the increase of the wall roughness and the reduction of the internal diameter. The device known as "pig" is driven through the pipe by the flow of oil, scraping deposits from the pipe wall as it travels and is used to perform "pigging" operations. Pigging has been widely studied in the past few decades.

McDonald & Baker (1964) derived the first mathematical model on pigging. The model, valid for spherical pigs, was meant to be used for prediction of the liquid hold-up. Barua (1982) improved the model by removing some limiting assumptions and by considering the slug acceleration.

Kohda et al. (1988) proposed the first two-phase transient pigging model based on correlations. Minami & Shoham (1995) used a mixed Eulerian-Lagrangian approach to couple the transient two-phase flow with the pig motion. Hosseinalipour et al. (2007b) followed a similar approach, testing a transient model and comparing the results against experimental data.

Azevedo et al. (1996) developed an algebraic, 1D, hydrodynamic model to describe the bypass pig dynamics. The model coefficients were determined through two-dimensional (2D) Computational Fluid Dynamics (CFD) simulations of a Newtonian, incompressible fluid flowing in steady state conditions. The $k - \epsilon$ model was employed for the simulations.

Lima et al. (1998) and Lima et al. (1999) modeled the liquid removal operation in a gas pipeline. The 1D two-phase model has been solved via a semi-implicit finite difference scheme and the results have been successfully compared with experimental data. Nguyen et al. (2001b) solved the gas mass and momentum equations by using the method of characteristics (MOC) and the Runge-Kutta method. Nguyen et al. (2001c) and Nguyen et al. (2001d) applied the model to a bypass pig case, Nguyen et al. (2001a) to a curved pipe case, and Kim et al. (2003) experimentally verified the model.

Nieckele et al. (2001) developed a single phase fluid model, taking into account wall deformations, and coupled it with the pig momentum equation. A similar approach has been followed by Hosseinalipour et al. (2007a) to simulate the pig motion in gas pipelines.

Xu & Gong (2005) developed a simplified pigging model to predict the pigging operation in gas-condensate horizontal pipelines with low liquid-loading. The model has been successfully compared with the OLGA code results. Tolmasquim & Nieckele (2008) developed a numerical code to simulate the transient oil flow in a pipeline during pigging operations and the results have been compared with field data.

In some works, the pig dynamics in dry conditions (no fluid flow) has been investigated. Hu & Appleton (2005) developed a dynamic model for a novel pig, designed to move both upstream and downstream, and verified the results against experimental data. Saeidbakhsh et al. (2009) analyzed the dynamics of small pigs in complex-shaped pipelines. The effect of the flow field was modeled by a time dependent force acting on the pig. The influence of the flow field was successively introduced. The fluid was considered incompressible by Lesani et al. (2012) and compressible by Mirshamsi & Rafeeyan (2015). In these three works, the dynamics of the system has been solved via a single ordinary differential equation.

Esmaeilzadeh et al. (2009) used the MOC to model the transient motion of a pig through liquid and gas pipelines. The simulation results showed good agreement with the gas-liquid pipeline field data. Deng et al. (2014) used the MOC to study the problem of column separation in gas-liquid pipelines during pigging operations. The simulation results were in good agreement with the field data.

Despite many models have been developed to describe the pig dynamics, most of them deal with gas flows and some of them with liquid removal in gas pipelines. In addition, all the cited models are limited to 1D domain. Waxy oils (wax-particles in oil mixture) in pipelines have been largely studied. Most of the literature focuses on two aspects: wax deposition in oil pipelines (Aiyejina et al. (2011)), and wax removal from pipelines wall (Lima et al. (1995)). Wang et al. (2005) studied the mechanics of wax removal in pipelines in dry conditions, while Wang et al. (2008) repeated the experiments with the oil flowing in the test facility. The tribological behavior of waxy oil subject to pipeline pigging has been investigated in the past few years using the fluorescence technique by Tan et al. (2014, 2015a) and with the portable microscopy technique by Tan et al. (2015b).

A few mathematical models tackle the the wax removal from pipeline walls. An example is the one developed by Azevedo et al. (1999) and experimentally verified by Barros Jr et al. (2005). Other pigging models, based on experimental results, have been developed to predict wax deposition (Wang

& Huang (2014)) and removal in pipelines (Huang et al. (2016)). Wang et al. (2015) studied experimentally the influence of several parameters on the wax breaking process in order to determine the optimal de-waxing frequency and evaluating the pigging risks. A good review illustrating the forces acting on a bypass pig in operation was written by Galta (2014) .

A few models studying the forces involved in the wax-removal process have been developed based on a mixed experimental-numerical procedure. In particular, Braga et al. (1999) considered the wax deposit as a linear elastic material and neglected the fluid flow, while Southgate (2004) included the oil flow, but considered the wax deposit as rigid and part of the pipe wall. The multiphase wax-oil flow in pipelines during pigging operations has been scarcely studied. An example is the 1D model developed by Hovden et al. (2003) with the OLGA 2000 code, where three different wax deposition models have been tested.

In this paper, a series of three-dimensional (3D) CFD simulations describing the interaction of the waxy oil with the moving pig are presented. Simulating the 3D flow is computationally demanding but has a two-fold advantage compared to the 1D approach: (i) it increases our understanding of the phenomenon, as it allows the visualization of the interaction between the pig surface and the wax chips; (ii) the results are less affected by modeling approximations.

2. Mathematical Modeling

In this section, the mathematical model describing the dynamics of the oil-wax system in a pipeline, subject to pigging operations, will be illustrated.

2.1. Pig Model

The main problem in representing the 3D pig motion numerically is due to the computational grid which must be warped in order to represent the pig displacement. Even though this can be realized with modern computational techniques, it is a computationally demanding operation.

A more convenient approach is to solve the problem in a frame of reference fixed to the pig center of mass, instead to an external observer, as done by Minami & Shoham (1995); Hosseinalipour et al. (2007b); Nieckele et al. (2001); Tolmasquim & Nieckele (2008) for 1D modeling. This is possible when the pipeline is straight, with a constant section, and the process is not investigated close to the pumping station or the outlet. Under these

conditions, the computational domain does not change as the time goes by. As the pig advances, the wax is scraped to accumulate in front of the pig. Despite the debris field grows in time, it only occupies a small portion of the pipeline.

The relationship between the velocity in the absolute frame of reference, $\vec{v}_a$, and the one in the relative frame of reference, $\vec{v}$, is

$$\vec{v} = \vec{v}_a - \vec{v}_{pig} \tag{1}$$

where $\vec{v}_{pig}$ is the pig velocity. In order to determine this parameter, two hypothesis were introduced: the pig under investigation is of *sealing* type, i.e. no flow between the two sides of the pig, and the oil flow rate,

$$Q_{oil} = \int_{A_{pipe}} \vec{v}_{a,oil} \cdot \hat{n} dA \tag{2}$$

is constant. The mean oil velocity upstream the pig, U, is defined as

$$U = \frac{4Q_{oil}}{\pi D^2_{pipe}} \tag{3}$$

In order for the mass to be conserved at the interface between the up-stream oil and the pig, it must be

$$v_{pig} = U \tag{4}$$

Eq.(4) can be written because the sealing pig has only one degree of freedom (1DOF), therefore: $v_{pig} = \vec{v}_{pig} \cdot \hat{n}$. In general, the pig could also spin around its axis. Nevertheless, the friction against the wall has been assumed high enough to prevent this. Since the oil flow rate is supposed to be constant, the pig velocity should be constant as well, by virtue of Eq.(4), therefore the pig inertial force, will not influence the dynamics of the oil-wax system. This is a reasonable approximation as the pig is most effective when it advances at a nearly constant, but not too high, speed as reported by Nguyen et al. (2001a); Esmaeilzadeh et al. (2009); Deng et al. (2014).

The pig operation is performed when the wax layer reaches a certain thickness h_{ip}. Normally, for security purposes, h_{ip} is very small compared to the pipe diameter. In order to represent this, the computational grid thickness should be of the same order of the deposit thickness, resulting in a large computational cost.

Supposing that the wax is uniformly distributed in the circular pipe, and it is pushed along the pig axis at the pig velocity, the flow rate of scraped wax during the pigging operation is given by:

$$Q_{wax} = \frac{\pi}{4} v_{pig} \left(D_{pipe}^2 - (D_{pipe} - 2h_w)^2 \right) \tag{5}$$

where Q_{wax} is the flow rate of the scraped wax. The pig-wax interfacial area, which is Q_{wax}/v_{pig}, is calculated as the wax removal efficiency was 100%, though in reality is always smaller. Nevertheless, this approximation is widely used to model the pig-wax deposit contact force, e.g. Braga et al. (1999); Barros Jr et al. (2005); Galta (2014), and it is used here to promote the slurry formation in a short time.

In order to reduce the computational cost, the effect of the scraped wax was embedded in a new boundary condition. A small area on the pipe surface called *injection area* has been introduced, where a positive flow rate of scraped wax corresponding to Q_{wax}, is imposed. Calling v_{inj} the velocity of the injected wax, and h_{inj} the injection area thickness, the flow rate of scraped wax reads:

$$Q_{wax} = v_{inj} \pi D_{pipe} h_{inj} \tag{6}$$

therefore,

$$v_{inj} = v_{pig} \frac{h_w}{h_{inj}} \left(1 - \frac{h_w}{D_{pipe}} \right) \tag{7}$$

In the moving frame of reference, the axial velocity is zero for the pig and the injection area, while in the rest of the pipe wall it is equal to $-v_{pig}\hat{x}$, where $\hat{x}$ is the unit vector in the direction of the pipe axis.

2.2. Physical Properties of the System

The debris field in front of the pig is composed of cut wall wax (gel) and oil. The debris field can be considered as a slurry of cut wall wax and oil with variable cut wax content dependent on the wall wax-pig-pipe flow dynamics.

The physical properties of oil and wax-in-oil slurry are temperature dependent. They have been derived experimentally, and are illustrated in Fig.(1), where the dependence of the slurry dynamic viscosity on temperature Fig.(1,a) and wax volume fraction Fig.(1,b), are shown. In Fig.(2), the density Fig.(2,a) and the viscosity Fig.(2,b) of the oil are shown. As Fig.(1) suggests, the pour point of the deposit-contaminated oil is below $-25F$.

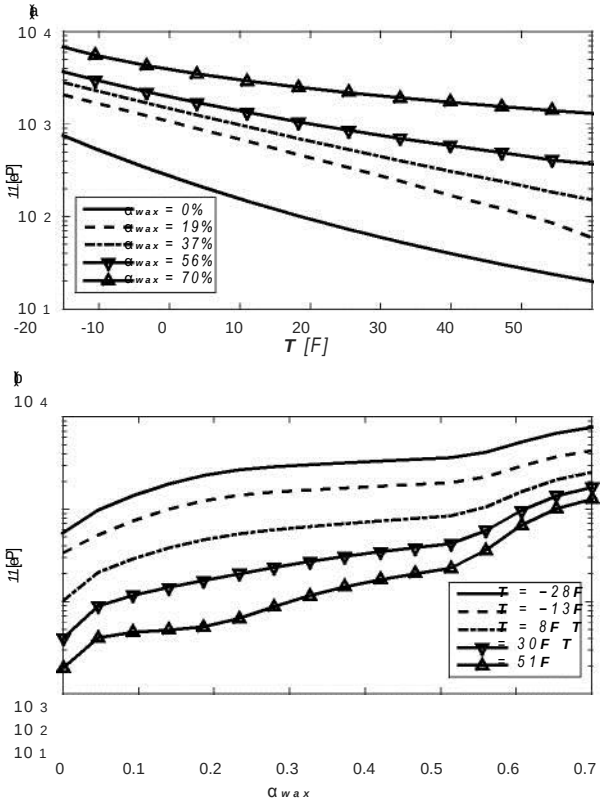

Figure 1: Dynamic viscosity of the wax-in-oil slurry: (a) vs Temperature; (b) vs Volume Fraction.

2.3. Fluid dynamic model

The flow of the mixture has been simulated with the *drift flux* model, which is widely used in multiphase modeling (Aarsnes et al. (2016); Varadarajan & Hammond (2015); Bhagwat & Ghajar (2014); Chen et al. (2012); Asheim & Grødal (1998); Gavrilyuk & Fabre (1996); Fran¸ca & Lahey (1992); Clark et al. (1990)), and solves the conservation of mass, momentum and energy of the mixture only. This implies that the momentum of each phase is not calculated explicitly and the inter-phase phenomena, such as settling, require modeling. In addition, a transport equation for the volume fraction of each phase is provided. In this work, the wax-in-oil slurry flow is considered to be laminar. This can be achieved if the pipe diameter is sufficiently small, because of the high wax viscosity. Moreover, the flow has been considered isothermal and therefore the energy equation has not been considered.

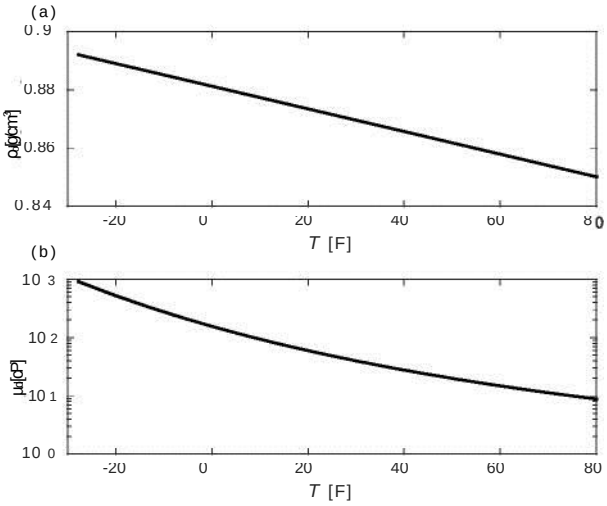

Figure 2: Oil properties: (a) density; (b) dynamic viscosity

177 The reduced pipe diameter and length limit the surface of heat exchange,
178 justifying that this assumption is valid if the observation time is small and
179 is suitable for non-heated pipelines.

180 The wax volume fraction in the slurry, a_{wax}, is defined as:

$$\alpha_{wax} = \frac{V_{wax}}{V_{rev}} \tag{8}$$

where V_{rev} is the Representative Volume Element (REV) which is the
181
182 smallest volume over which a measurement can be made that will yield a
183 value representative of the whole. Since in the domain of investigation there
184 are only oil and wax particles, the following relationship applies:

$$\alpha_{oil} = 1 - \alpha_{wax} \tag{9}$$

185 The continuity equation for the wax phase can be written as:

$$\frac{\partial}{\partial t}(\rho_{wax}\alpha_{wax}) + \mathrm{div}\,(\rho_{wax}\alpha_{wax}(\alpha v_m + \alpha v_{d_w})) = 0$$

186 where

$$\alpha v_{dw} = \alpha v_{wax} - \alpha v_m \tag{11}$$

is the drift velocity,

$$\square_m \qquad (12)$$

the mixture velocity, and,

$$\square_m = \square_{oil}\square_{oil} + \square_{wax}\square_{wax} \qquad (13)$$

the mixture density. Adding up the mass conservation of each phase, e.g. Eqs.(9,10), the conservation of mass for the mixture can be obtained as:

$$\frac{\partial \square_m}{\partial t} + \operatorname{div}(\square_m \square v_m) = 0 \qquad (14)$$

The mixture momentum equation can be written as

$$\frac{\partial}{\partial t}(\square_m \square v_m) + \operatorname{div}(\square_m \square v_m \otimes \square v_m) = -\nabla p_m + \operatorname{div}([\square_m] + [\square_{dm}]) + \square_m \square g \qquad (15)$$

where p_m is the mixture pressure, or just pressure,

$$[\square_{dm}] = \square_{oil} \square \; {}^{\square} v_{dw} \otimes {}^{\square} v_{dw} \qquad (16)$$

is the *drift stress tensor*, and

$$[\square_m] = \mu_m(T, \square_{wax})\left[\nabla \square v_m\right] + \left[\nabla \square v_m\right]^T - \tfrac{2}{3}\operatorname{div}(\square v_m)[I] \qquad (17)$$

the *viscous stress tensor* with $[I]$ the identity tensor and $\mu_m(T, \square_{wax})$ the mixture viscosity which, as can be seen from the experimental data in Fig.(1), is a function of both the temperature and the wax volume fraction. Further details on the Drift Flux Model can be found in Rusche (2003).

As it can be seen from Eqs.(10,16,17), the model is complete once the expression of the drift velocity and mixture viscosity are supplied.

2.4. Mixture Viscosity Model

The mixture viscosity has been derived experimentally and the results are shown in Fig.(1). The slurry viscosity was measured in a rotational vane rheometer at constant constant shear rate of $301/s$ as the temperature was reduced uniformly from the wax appearance temperature ($80F$) to $-28F$

Table 1: Coefficients of the Mixture Viscosity Model

$T(F)$	b_1	b_2	b_3	b_4	r^2
-25	7.9805	-3.342	2.1055	0.48004	0.9770
0	18.516	-7.3499	3.1263	0.38464	0.9905
25	18.583	-6.515	3.3366	0.53254	0.9790
50	8.9526	-1.7972	3.4096	0.63734	0.9490

over 18 hours. The measurement have been performed at varying volumetric fractions of cut wax. At each temperature, the mixture viscosity shows a discontinuous slope for $\phi_{wax} = 0.5$, appearing to reach an asymptote near $\phi_{wax} = 0.7$, which is the maximum packing fraction. This is consistent with the change of particle arrangement. For $\phi_{wax} < 0.5$ the wax chips are more free to move and their orientation is random; above this value the chips start packing and the mixture viscosity increases abruptly. In order to fit the experimental data, the following relationship is introduced:

$$\ln \frac{\mu_m(T, \phi_{wax})}{\mu_m(T, 0)} = \max\left(\frac{b_1(T)\phi_{wax}}{1 - b_2(T)\phi_{wax}^{1} - b_4(T)\phi_{wax}}, b_3(T)\phi_{wax} \right) \quad (18)$$

In Tab.(1) the b_i coefficients, along with the square correlation coefficient r^2, which shows how well the model in Eq.(18) reproduces the experimental results, are reported. It must be noted that the value $\mu_m(T, 0)$ is not in that table, because it corresponds to the oil viscosity and will be shown in Tab.(3)

2.5. Drift Velocity Model

The Stokes' velocity, which is the terminal velocity o

$$v_s = \frac{1}{18}$$

laminar regime, reads:

$$\frac{(\rho_{wax} - \rho_{oil})\, g d_{wax}^2}{\mu_{oil}}$$

In case of hindered settling, an alternative expression has been proposed by Camenen (2008)

$$v_{hs} = v_{wax} v_{oil} = v_s \left(1 - \frac{\phi_{wax}}{\phi_{wax,\max}}\right)^{\omega\alpha\xi,\max} \quad (20)$$

Table 2: Settling velocity

$T(F)$	$d_{wax}(mm)$	$v_s(mm/s)$	Re_p	n
-25	2	-0.251	$5.8 \cdot 10^{-4}$	4.6
0	2	-1.369	$1.5 \cdot 10^{-2}$	4.6
25	2	-4.857	$1.7 \cdot 10^{-1}$	4.6
50	2	-12.97	1.1	4.35
-25	0.4	-0.010	$4.6 \cdot 10^{-6}$	4.6
0	0.4	-0.055	$1.2 \cdot 10^{-4}$	4.6
25	0.4	-0.194	$1.4 \cdot 10^{-3}$	4.6
50	0.4	-0.519	$8.9 \cdot 10^{-3}$	4.6

where $\phi_{wax,\max}$ is the maximum volume fraction, which in this work has been assumed equal to 0.7, and n is an exponent defined as

$$n = \begin{cases} 4.6 \text{ for } Re_p < 0.2 \\ 4.4 Re_p^{-0.03} \text{ for } 0.2 < Re_p < 1 \\ 4.4 Re_p^{-0.1} \text{ for } 1 < Re_p < 500 \\ 2.4 \text{ for } Re_p > 500 \end{cases} \quad (21)$$

where Re_p is the particle Reynolds number defined as

$$Re_p = \frac{\rho_{oil} |v_s| d_{wax}}{\mu_{oil}} \quad (22)$$

The settling velocity in Eq.(20) has been validated against experimental data on particles of different shapes and dimensions (Camenen (2008)). Therefore, in this context the particle diameter is the largest distance between two points of the particle.

Finally, the drift velocity reads:

$$v_{dw} = \frac{\rho_{oil} \phi_o}{\phi_m} v_{hs} \quad (23)$$

In Tab.(2) the settling velocity values for different temperatures and particle diameters have been reported along with the particle Reynolds number and the exponent n appearing in Eqs.(20,22).

3. Materials and Method

The simulations have been performed using the `driftFluxFoam` solver, available in OpenFOAM v3.0, which solves the fluid dynamics equations with the Finite Volume Method (FVM) and uses the SIMPLE algorithm for the pressure-velocity coupling. The computational grid has been realized with the `blockMesh` utility of OpenFOAM v3.0. Only the pipe in front of the pig, which has a diameter of $3in$ and is 60 diameters long, has been considered as the domain of investigation, since a constant oil flow rate of $37 USgal/min$ has been imposed. These dimensions are not typical of oil pipelines but can be found in test facilities (Barros Jr et al. (2005); Team (2011); Wang et al. (2015); Huang et al. (2016)). The front pig wall is steady, because of the moving frame of reference, while the pipe wall is moving backwards at the pig speed. In order to ensure mass conservation, both pig and mean oil velocity are equal to $1.7 ft/s (0.51 m/s)$.

At the *injection area* only wax is present, with an injection velocity given by Eq.(7) and directed radially inwards. This condition represents the scraping of a 2mm thick wax deposit. The resulting flow rate of scraped wax is about $3.78 USgal/min$, regardless of the particle diameter. Therefore, the smaller the particles, the higher their number. Since the injection boundary condition, defined in Eq.(7), decouples the flow rate of scraped wax from the particle diameter, it is possible to study the influence of these two parameters separately.

The velocity normal derivative is set to zero at the outlet boundary (Neumann boundary condition). As far as the volume fractions are concerned, the normal derivative is set to zero everywhere except at the injection area, where a fixed volume fraction is imposed. This corresponds to zero mass flux at the boundary (Vorobev & Boghi (2016)).

Eight simulations have been set up. Four different temperatures, i.e. $-25F$, $0F$, $25F$, $50F$, and 2 particle diameters, i.e. $2mm$, $0.4mm$, have been investigated. The uniform particle diameter is an approximation made to study the effect of this parameter. In reality, during the scraping process, particles of different dimensions are injected into the pipe. The temperatures chosen are very low, and the particle diameters high. Nevertheless, these extreme conditions can be found in the trans Alaska pipeline system (Team (2011)) and have been chosen to provoke crystallization in a short length, and obtain a developed wax-in-oil slurry in a short model time.

4. Results

The simulations have been performed on the Astral Cluster with Xeon 5160 dual core processors at Cranfield University. Each simulation run on 32 processors and took approximately 4 hours and 40 minutes, on a grid made of 518400 hexaedra, to be completed.

The results are grouped in two categories: *Results at* 2*mm wax particle diameter*, and *Results at* 0.4*mm wax particle diameter*. The results will be expressed in terms of section averaged variables as well, since many pipeline codes provide them.

The wax area fraction is defined as:

$$\alpha_{wax}(t,x) = \frac{1}{\pi R_{200}} \int_{2/r} \int_{R} \alpha_{wax}(t,r,\theta,x) r dr d\theta \tag{24}$$

$$\alpha_m(t,x) = \alpha_{oil} + (\alpha_{wax} - \alpha_{oil})\,\alpha_{wax}(t,x) \tag{25}$$

the section averaged momentum is defined as:

$$\alpha_m(t,x) U_m(t,x) = \frac{1}{\pi R^2} \int_0^{1} \int_{2/r} \int_{0}^{R} \alpha_m(t,r,\theta,x) v_m(t,r,\theta,x) \cdot \hat{x} r dr d\theta \tag{26}$$

the section averaged pressure drop is defined as:

$$p(t,x) = \frac{1}{\pi R_{200}} \int_{2/r} \int_{R} p_m(t,r,\theta,x) r dr d\theta \tag{27}$$

For a single phase flow, the pressure drop can be calculated according to the following formula:

$$p_{oil}(t,x) - p_{out} = \rho_{oil} \left(\frac{4Q_{oil}}{2\pi D^2}\right)^2 \left(\frac{\lambda'}{} + \lambda(\mathrm{Re}_{oil}, \epsilon/D) \frac{L}{D} - x\right) \tag{28}$$

Where Q_{oil} is the mean oil velocity, D the hydraulic diameter and λ' is the local friction factor which takes into account the localized loss of charge due to the fact that the velocity profile at the pig surface is not fully developed (Al-Nassri & Unny (1981)). This coefficient has been derived by performing a

Table 3: Properties used for the simulations

$T(F)$	$p_{oil}(g/cm^3)$	$p_{wax}(g/cm^3)$	$\mu_{oil}(cP)$	$\mu_{wax}(cP)$	Re_{oil}	$\Delta p_{ref}(kPa)$
-25	0.891	0.98	771.71	7103.6	45	9.96
0	0.881	0.98	157.68	3150.5	218	2.03
25	0.871	0.98	48.92	2026.2	695	0.63
50	0.861	0.98	20.00	1487.7	1680	0.26

series of numerical simulations at different temperatures with only oil flowing in the pipeline, and its value has been found equal to 0.1 approximately for every temperature.

In Tab.(3) the properties used for the simulations have been reported. The density and viscosity values have been experimentally determined and have been shown in Fig.(1) and Fig.(2). It must be noted that $\mu_{oil} = \mu_m\ (T,\ a_{wax} = 0)$ and $\mu_{wax} = \mu_m\ (T,\ a_{wax} = 0.7)$. The last two values in Tab.(3) refer to the simulations in which only pure oil is flowing. As μ_{oil} is the minimum value for the mixture viscosity and Re_{oil} is the highest Reynolds number for the wax-in-oil slurry flow, the mixture flows in laminar regime. Moreover, Δp_{ref} is the pressure drop in the domain when only pure oil is flowing, and it is the lowest pressure drop which can occur in the domain.

4.1. Results at 2mm wax particle diameter

The cut wax volume fraction field is shown in Fig.(3). The solutions at different temperatures are compared. The volume fraction field appears to be more diffuse at lower temperatures. This is due to the fact that the oil viscosity increases with the decreasing temperature. This reduces the settling velocity v_s and increases the wax particles dispersion.

When the pig scrapes the wax deposit at $T = -25F$, the wax particles travel a relatively long distance, because of the small settling velocity. Therefore, at the bottom of the pipe a region can be observed, 40 diameters long and half a diameter high, in which the wax volume fraction is relatively low (35%). This will be called “lubrication region”, because it is characterized by a low viscosity, as Fig.(1) suggests.

At $T = 0F$ a lubrication region at the pipe bottom, 28 diameters long, can be observed as well. This region is shorter than the previous case but its wax content is higher (50%). A high wax content region can be seen downstream the lubrication region. Nevertheless, due to the low settling, its boundaries cannot be clearly defined. In this region, also present for $T = -25F$, the particles settle. Further downstream another low wax content region can be seen.

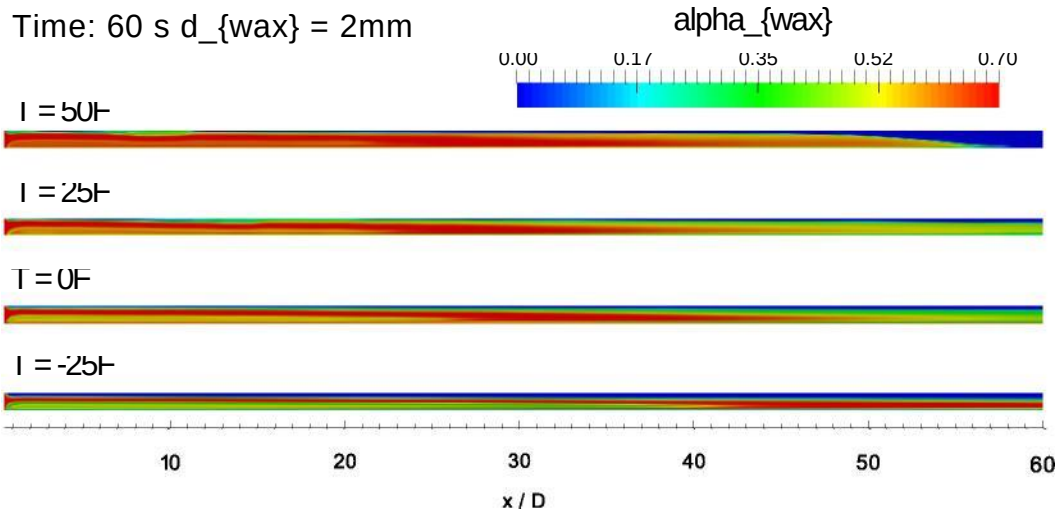

Figure 3: Wax volume fraction field for $2mm$ particle diameter at 60 seconds after the beginning of the process.

The wax debris field is similar to the previous cases for $T = 25F$ and $T = 50F$ with a shorter and more viscous lubrication region. A remarkable difference can be observed for $T = 50F$, where only pure oil can be seen downstream the high wax content region. This is due to the high settling velocity which promotes wax deposition.

In Fig.(4) the section averaged wax debris field, defined in Eq.(24), at different instants of time is shown. The stratified debris field assumes a "dune" shape. The wax distribution increases slightly in height compared to the length. This means that the height of the dune, is mostly set at the beginning of the operations. Therefore, the fluid dynamic conditions at the pig front surface must play an important role in determining this parameter.

It is interesting to compare the 3D information given in Fig.(3), with the

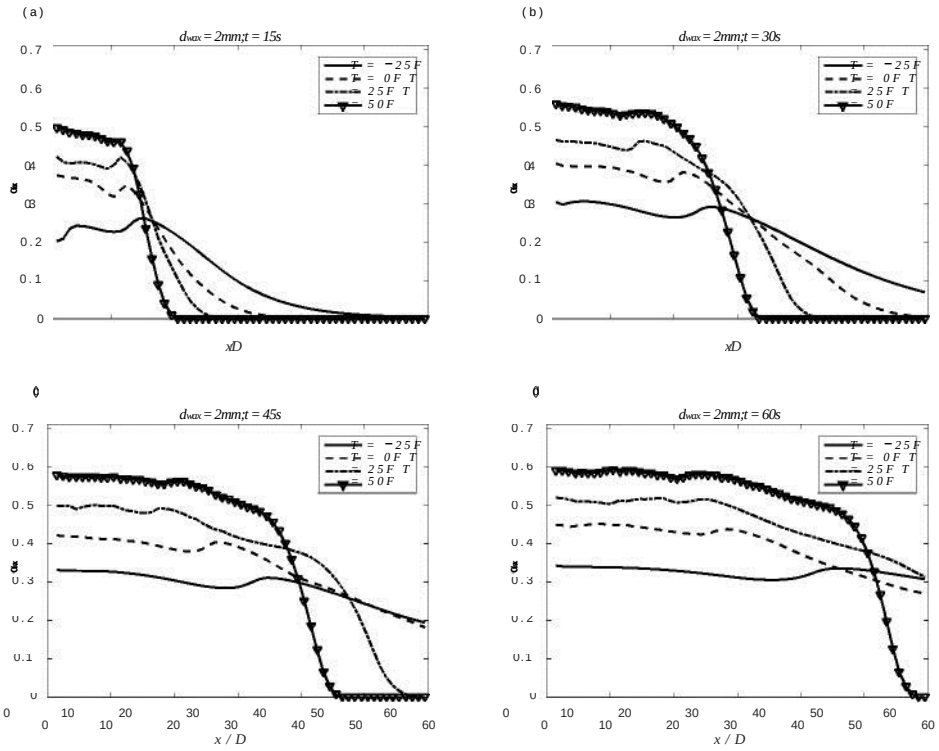

Figure 4: Section averaged cut wax volume fraction field for 2mm particle diameter. (a) t = 15s; (b) t = 30s; (c) t = 45s; (d) t = 60s.

1D in Fig.(4,d). The section average is more representative of the instantaneous field at higher temperatures because the debris distribution is more uniform. The presence of a lubrication region cannot be deduced from the 1D field.

For $_{awax}$ at $T = -25F$ the wax-in-oil slurry is stratified: the top layer contains 0% of wax (oil layer), the second layer contains about 70% of wax, and the bottom layer contains 35% of wax. However, it is not possible to retrieve this information from the section averaged field.

This is very important as the pressure drop across the pipe is influenced by the local viscosity that depends on the wax distribution. A simplified 1D model which does not take into account the wax distribution, risks to give an unreliable estimation of the pressure drop.

The time growth of the wax-in oil slurry is an interesting output for

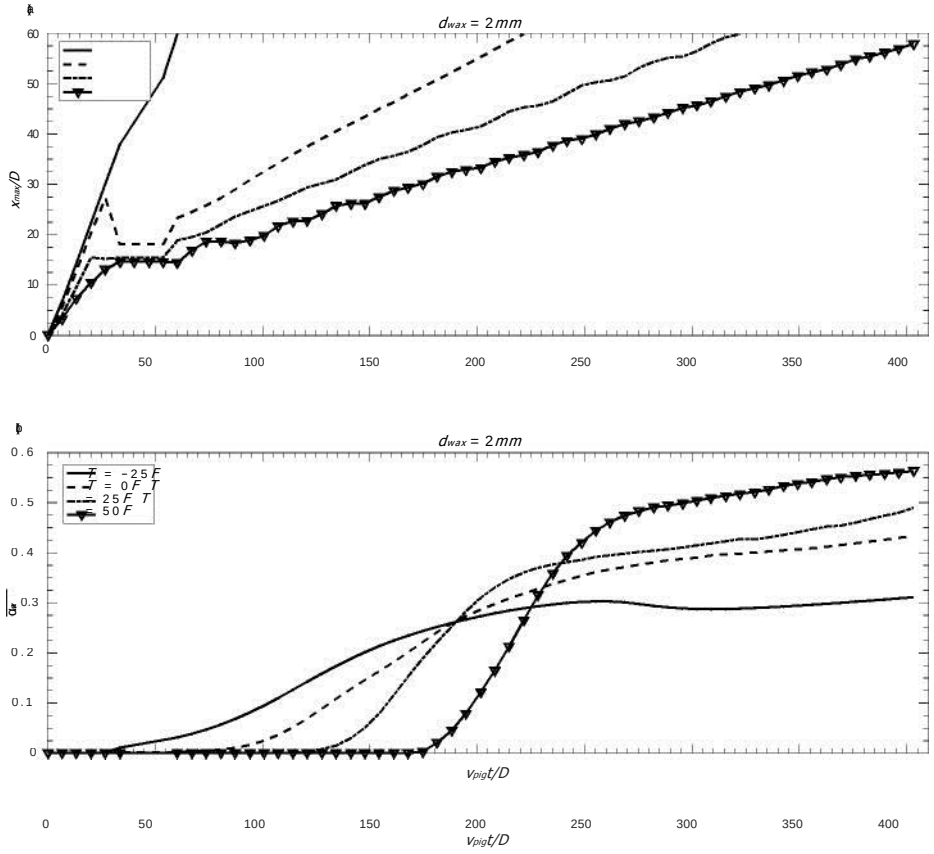

Figure 5: Time growth of wax-in-oil slurry for d_{wax} = 2*mm*. (a) wax-in-oil slurry length vs time; (b) wax volume fraction at *x/D* = 30 vs time.

the operators. The injection boundary condition, i.e. Eq.(7), for a sealing pig ensures that the wax debris content increases linearly in time for every temperature and particle diameter. Therefore, in Fig.(5,a) the growth of the wax-in-oil slurry length in time is shown, while in Fig.(5,b) the increase of wax volume fraction at *x/D* = 30 is shown. The time has been non-dimensionalized using the time scale D/v_{pig}. As far as the wax-in-oil slurry length is concerned, after an initial establishment period, the growth is essentially linear in time.

Moreover, the slope of the curve is inversely proportional to the temperature. This is due to the settling, which is higher at higher temperatures. As far as the wax volume fraction at *x/D* = 30 is concerned, the variables

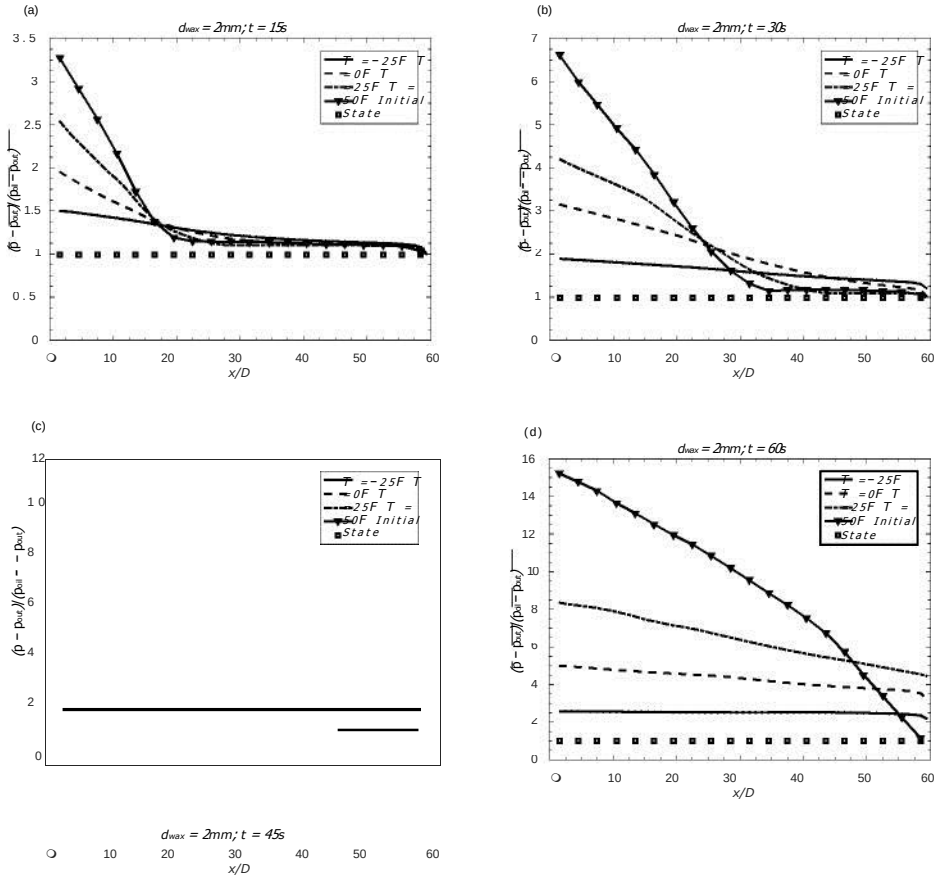

Figure 6: Ratio between the section averaged and the pure oil pressure drop for d_{wax} = 2mm vs axial distance. (a) t = 15s; (b) t = 30s; (c) t = 45s; (d) t = 60s.

undergo a phase of fast growth and then stabilize to a certain value. For lower temperatures the growth occurs earlier, but the final volume fraction is smaller. This is also due to the difference in settling.

The ratio between the section averaged pressure drop of the mixture, defined in Eq.(27), and the pure oil, defined in Eq.(28), is shown in Fig.(6). The aim of this variable is to show the increase in pressure drop due to the debris field. Despite the absolute pressure drop is lower at the higher temperatures, the pressure drop ratio is higher at higher temperatures.

This is due to the fact that the viscosity is inversely proportional to the temperatures. Therefore, the increase of pressure drop is more significant at higher temperatures compared to lower ones. Nevertheless, the increase in

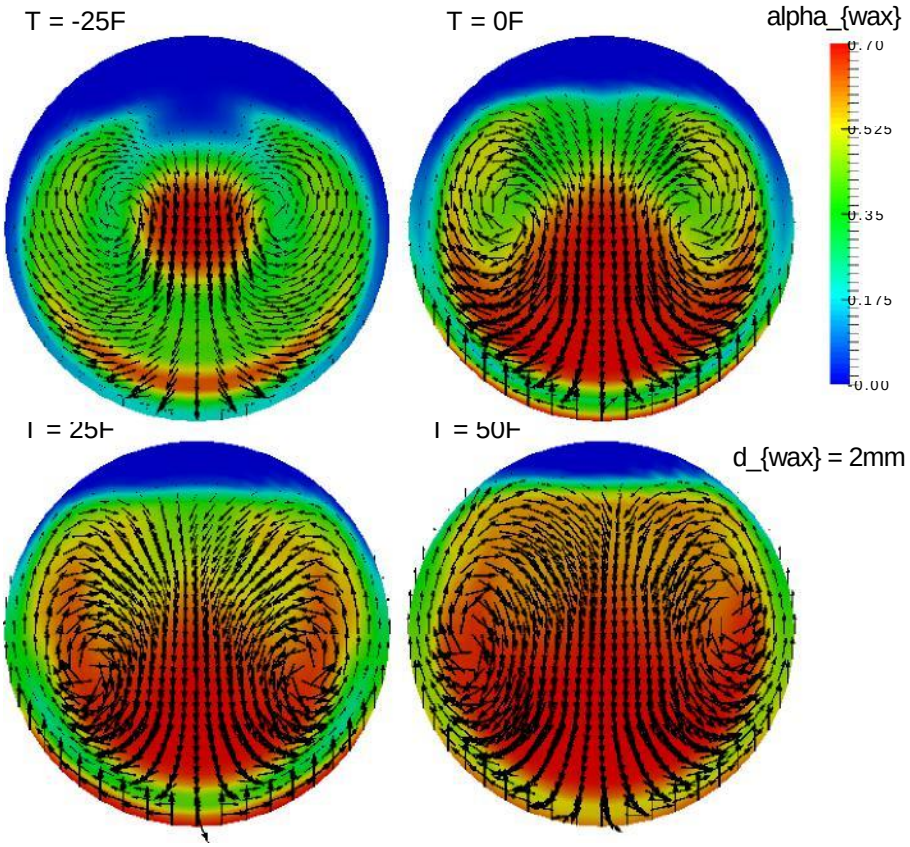

Figure 7: Cut wax planar velocity for d_{wax} = 2mm, t = 60s, x/D = 30

pressure drop due to the debris is not negligible at small temperatures, as it can be seen in Fig.(6) where at $T = -25F$, the pressure drop ratio is 2.5, while at $T = 50F$ it is 15.5.

In Fig.(7) the planar velocity vectors along with the wax volume fraction field are shown. The velocity vector pattern is highly dependent on the wax debris distribution. At each temperature there is a central region with a_{wax} = 0.7 surrounded by two counter-rotating vortexes. There is a crescent shaped region with a_{wax} = 0.7 towards the bottom. Close to the wall the wax volume fraction is lower, which is responsible for the lubrication effect. The wax chips move towards the bottom and the average volume fraction increases at higher temperatures, as it can be seen in Fig.(4).

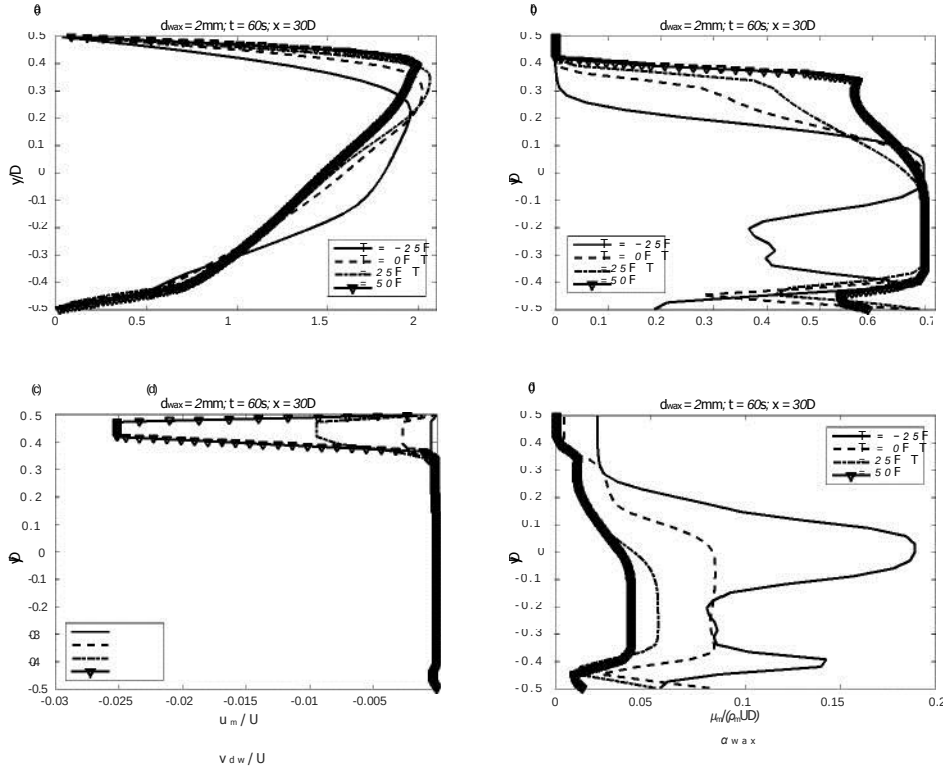

Figure 8: Profiles for d_{wax} = 2mm, 60 seconds after the beginning of the process and 30 diameters downstream the pig. (a) Normalized axial mixture velocity; (b) wax volume fraction; (c) Normalized vertical drift velocity; (d) Normalized Mixture Viscosity.

In Fig.(8,a) the mixture axial velocity scaled by the velocity U, defined in Eq.(3), is shown. The mixture axial velocity is highly dependent on the local mixture viscosity, shown in Fig.(8,d) which is scaled by $p_m UD$. The velocity gradient decreases with the increasing viscosity in order to ensure the continuity of shear stress at the boundary between the oil and the wax-in-oil slurry. As the temperature increases, the maximum velocity moves towards the pipe top wall because of the higher wax content at the bottom. In Fig.(8,c) the drift velocity scaled by U is shown. The drift velocity increases in the oil region, in agreement with Eq.(20), and decreases with the increasing temperature, in agreement with Eq.(19).

4.2. Results at 0.4mm wax particle diameter

The wax debris field in the middle section of the pipe, with a particle diameter of 0.4*mm*, is shown in Fig.(9). There is an increase in dispersion compared to the previous case. This is in agreement with Eq.(19), which reduces the settling velocity 25 times, compared to the previous case.

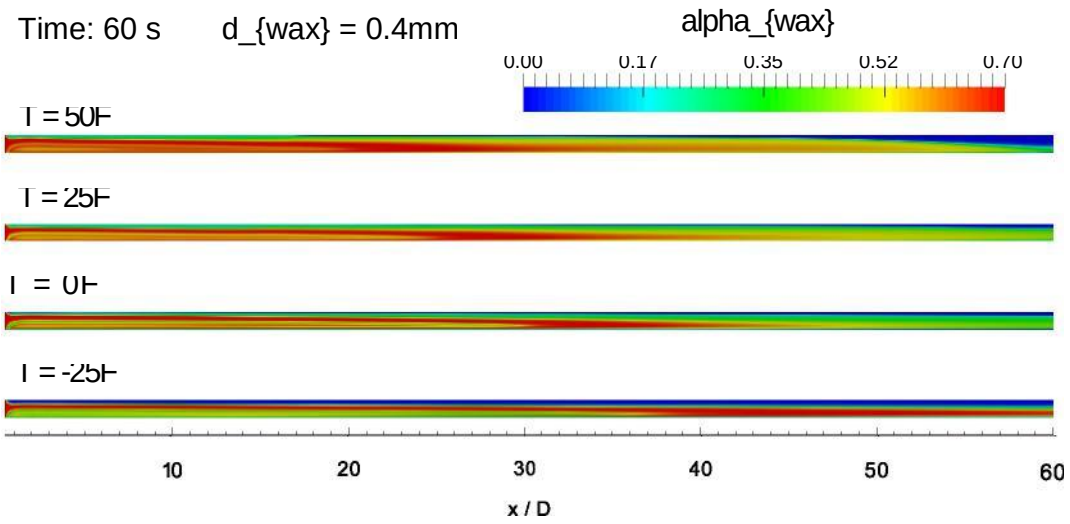

Figure 9: Wax volume fraction field for 0.4mm particle diameter at 60 seconds after the beginning of the process.

At $T = -25F$ the results are very similar with those shown in Fig.(3) because in both cases the drift velocity is small enough to keep the particles in suspension. For the other temperatures, some differences with the previous case can be observed at the end of the domain. The near field is characterized by a layered structure previously observed in Fig.(3). The particle diameter seems to influence the particle deposition mostly in the far-field. This suggests that the morphology of the debris field is mostly determined by the temperature.

The reason for this behavior is in the nature of the settling process, which is faster in pure liquids, and slower in slurry. Therefore, the differences between Fig.(3) and Fig.(9) are more evident in the far-field, because the particles fall in the oil and the difference between the settling velocities is not negligible, while in the near-field the particles fall in the wax-in-oil slurry and in both cases the settling velocity is very small.

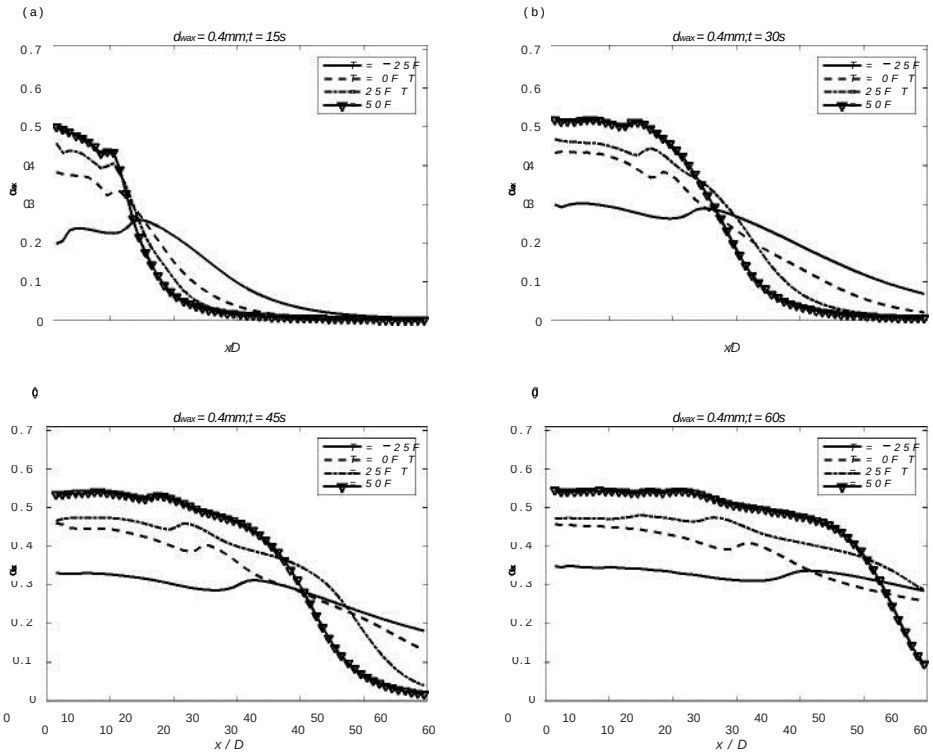

Figure 10: Section averaged cut wax volume fraction field for 2mm particle diameter. (a) t = 15s; (b) t = 30s; (c) t = 45s; (d) t = 60s.

In Fig.(10), the section averaged wax fraction at different time instants and temperatures is shown. In this case, the differences between the volume fraction field and the section averaged are less evident because the debris are more dispersed. However, the average does not show the stratification in Fig.(9) both in this case as well as in the previous one. The loss of this information could lead to a wrong estimate of velocity gradient and pressure drop.

The profiles in Fig.(10) and Fig.(4) appear to be very similar, with few differences. For d_{wax} = 0.4mm, the wax fraction is more uniformly distributed in the pipe compared to d_{wax} = 2mm. For d_{wax} = 0.4mm, the averaged wax fraction is lower in the near field and higher in the far-field as compared to d_{wax} = 2mm. This is due to the lower settling velocity which allows the particles to travel further downstream the pipe.

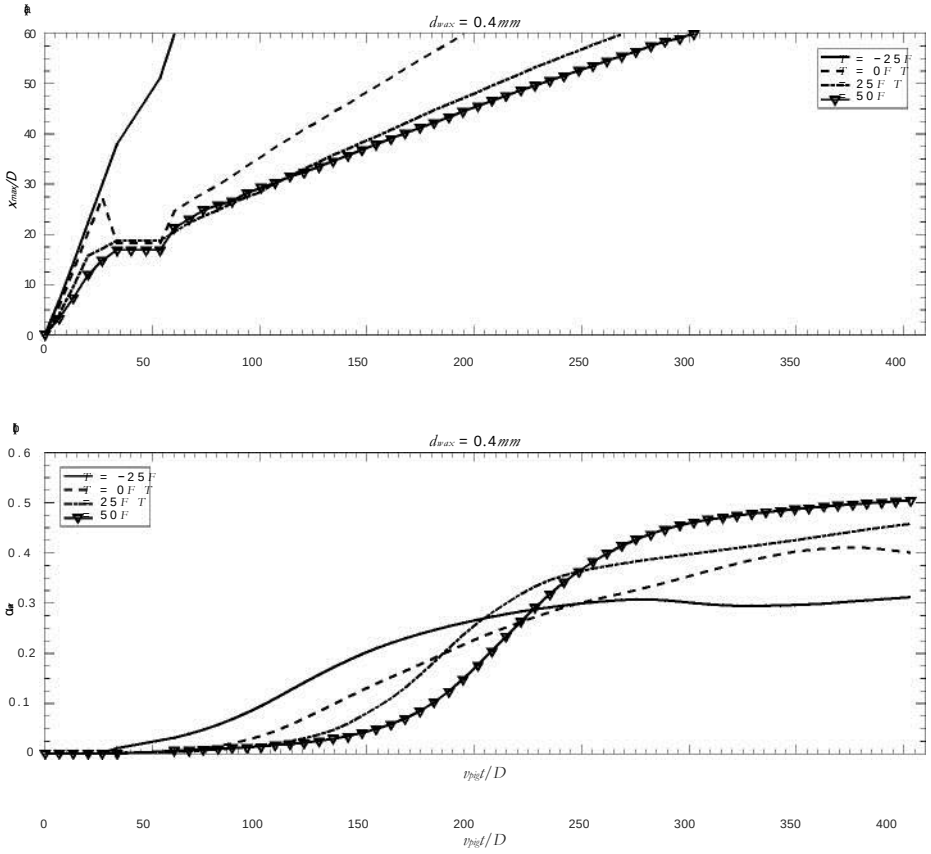

Figure 11: Time growth of wax-in-oil slurry for d_{wax} = 0.4mm. (a) wax-in-oil slurry length vs time; (b) wax volume fraction at x/D = 30 vs time.

In Fig.(11,a) the growth of the wax-in-oil slurry length in time is shown, while in Fig.(11,b) the increase of wax volume fraction at *x/D* = 30 is shown. The time has been non-dimensionalized using the time scale *D/vpig.* As for the previous case, the growth is essentially linear in time with the slope of the curve inversely proportional to the temperature. Comparing Fig.(11,a) with Fig.(5,a) it can be seen that the growth is quicker for $d_{wax} = 0.4mm$ due to the lower settling.

As far as the wax volume fraction at *x/D* = 30 is concerned, comparing Fig.(11,b) with Fig.(5,b) it can be seen that for every temperature the growth occurs earlier, but the final volume fraction is smaller, which is also due to the reduced settling.

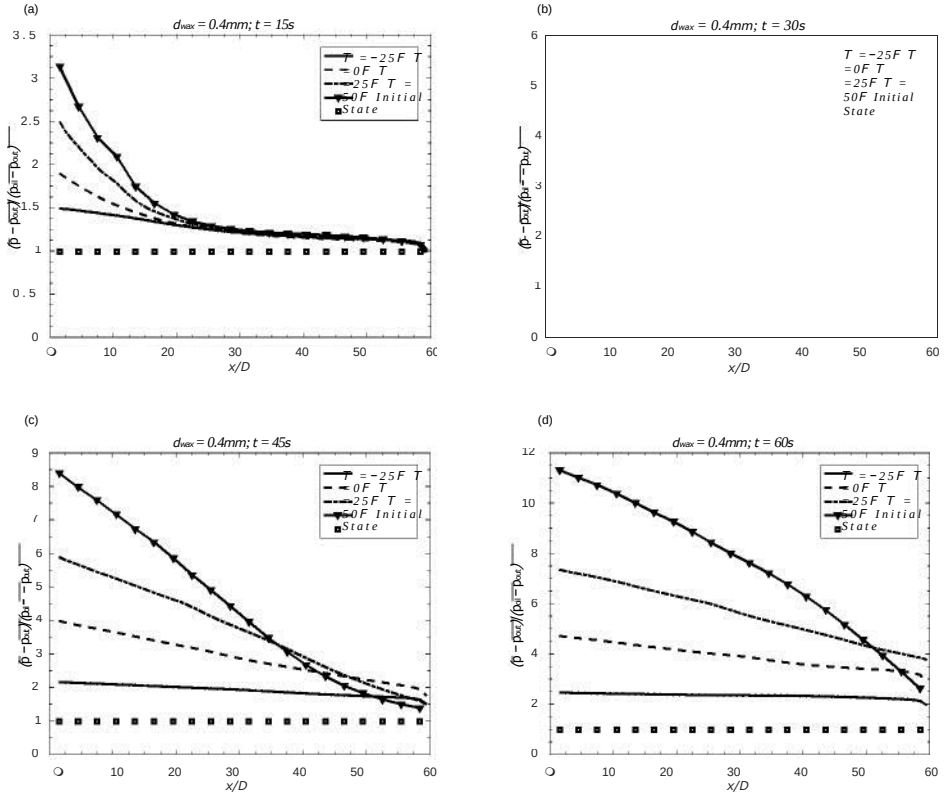

Figure 12: Ratio between the section averaged and the pure oil pressure drop for d_{wax} = 0.4mm vs axial distance. (a) t = 15s; (b) t = 30s; (c) t = 45s; (d) t = 60s.

In Fig.(12),the ratio between the section averaged pressure drop of the mixture and the pure oil, is shown. This variable is obtained from the ratio between the expressions in Eq.(27) and Eq.(28). Comparing the profiles in Fig.(12) and Fig.(6), it can be seen that, in analogy with the previous case, the pressure drop increases in the presence of debris. Nevertheless, this effect is less pronounced as compared to Fig.(6). We can conclude that the pressure drop decreases for decreasing particle diameters. From this result, we can hypothesize that any mechanism promoting particle breakage, as a jet for instance, may reduce the pressure drop.

In Fig.(13) the planar velocity vectors along with the wax volume fraction field are shown. In general, the motion is more dispersed as compared to the

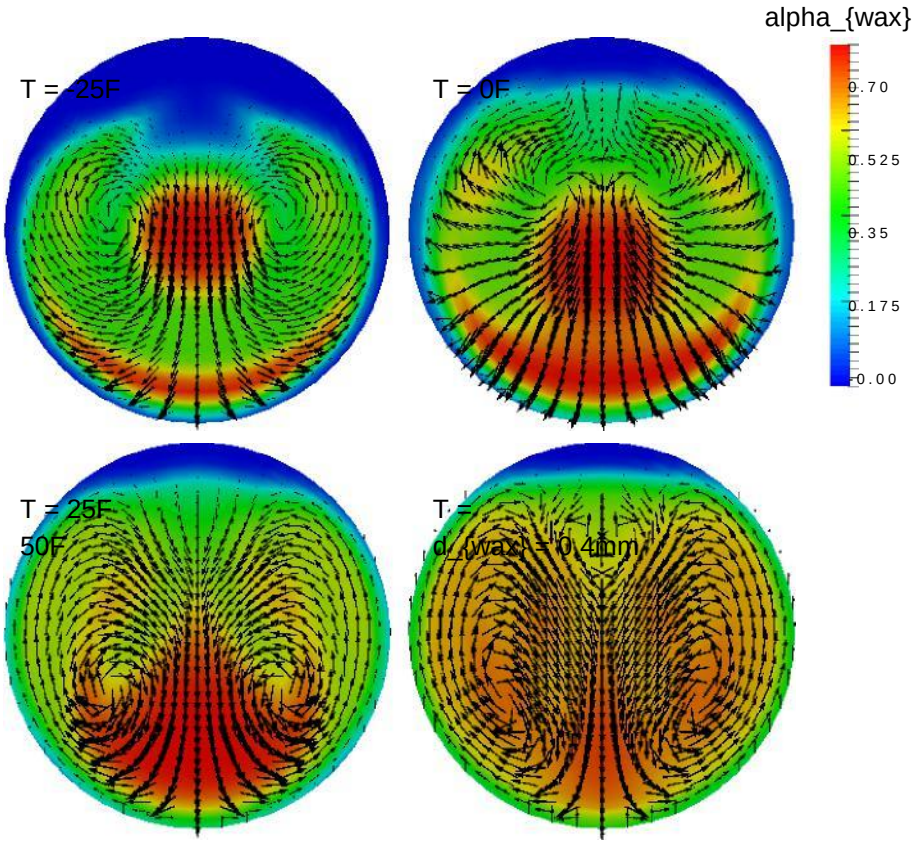

Figure 13: Cut wax planar velocity for d_{wax} = 0.4mm, t = 60s, x/D = 30.

previous case. For $T = -25F$, the particle diameter has scarce influence on the solution. For the other temperatures some differences with the previous case can be observed: the wax content is lower, as it can be deduced by comparing Fig.(10) with Fig.(4), and the counter-rotating vortexes are closer to the top of the pipe. At $T = 50F$, the velocity fields for the $d_{wax} = 2mm$ and $d_{wax} = 0.4mm$ appear very different. For $d_{wax} = 0.4mm$ the vortexes are in the lower part of the pipe and their major axes are inclined with respect to the vertical axis of $\pm ir/4$. For $d_{wax} = 2mm$, the vortexes are located at the center of the section and their major axes are parallel to the vertical axis.

In Fig.(14,a), the mixture axial velocity, scaled by the velocity U, defined in Eq.(3), is shown. Comparing this result with Fig.(8,a) it can be seen that

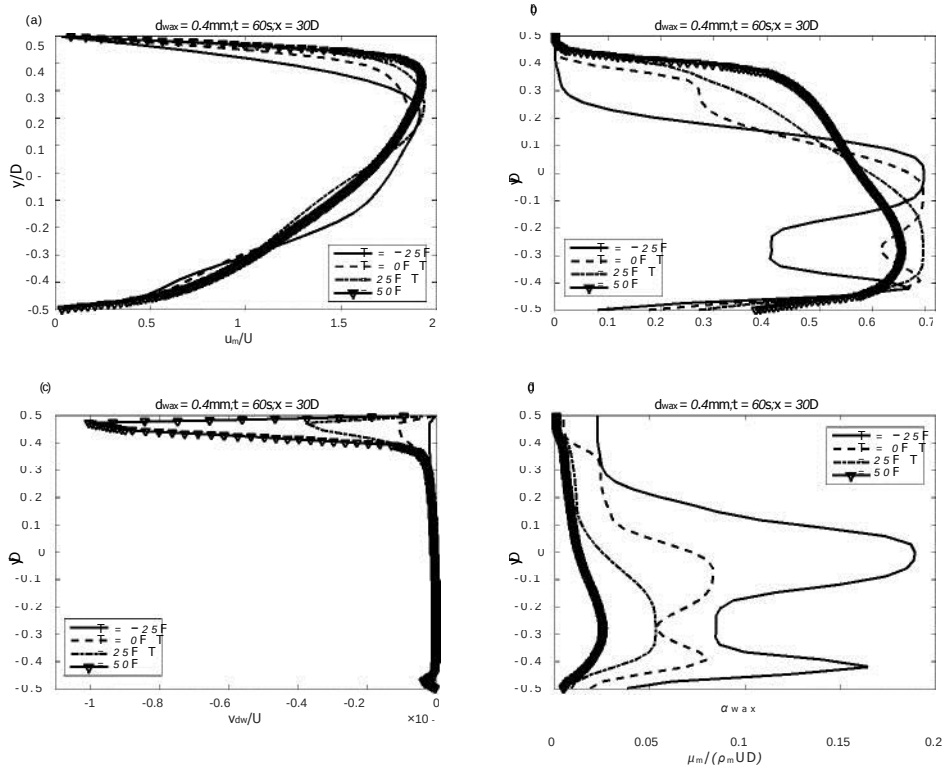

Figure 14: Profiles for d_{wax} = 0.4mm, 60 seconds after the beginning of the process and 30 diameters downstream the pig. (a) Normalized axial mixture velocity; (b) wax volume fraction; (c) Normalized vertical drift velocity; (d) Normalized Mixture Viscosity.

the profiles are smoother and the maximum velocity is lower. This is due to the fact that the wax distribution is more uniform and therefore the viscosity profile is smoother, as it can be seen comparing Fig.(8,d) with Fig.(14,d). The variable which is mostly influenced by the particle diameter is the drift velocity since is proportional to the settling velocity. Comparing Fig.(8,c) with Fig.(14,c) it can be seen that the two profiles have a similar shape, with the maximum in the oil region and decaying to zero for $_{awax}$ 0.7. Furthermore, in agreement with Eq.(19), the drift velocity maximum is 25 times smaller for d_{wax} = 0.4mm as compared to d_{wax} = 2mm.

5. Discussion

The results of the present 3D numerical investigation reveal some important details about the debris flow, which could not be derived from 1D analysis. Comparing Fig.(3) with Fig.(4), and Fig.(9) with Fig.(10), it can be seen that the 1D information is more representative of the 3D debris field at high temperatures, e.g. T = 50F. At lower temperatures, the information concerning the stratification are lost.

The results of Fig.(3) and Fig.(9) show that the temperature has a greater influence on the debris field than the particle diameter. In agreement with Eq.(19), the debris field is more dispersed for lower temperatures and particle diameters. In this work the mixture flows in laminar regime, however, in larger pipelines turbulence is an important factor (Patrachari & Johannes (2012)). At higher Reynolds numbers, the competition between turbulence and settling could keep the particle in suspension and it is unclear if small enough debris remain suspended. Answering this question is beyond the purpose of this work, however, the results in Figs.(7,13), show that, in the pipe cross-section there is a whirling motion which favors particle deposition. Moreover, the unsteady 3D results show a very similar debris distribution for the different particle diameters.

Despite the fact that turbulence may occur for higher oil flow rates, the high wax-in-oil slurry viscosity is likely to restore the laminar flow over time. In presence of a stratified flow, pure oil flows in a narrow section at the top of the pipe. From the results in Fig.(8,a) and Fig.(14,a) it is clear that the oil flow is laminar. The oil speed can play an important role in the determination of the height of the wax-in-oil slurry, which has a “dune” shape. Comparing Fig.(4) and Fig.(10), it can be seen that the height of the dune is proportional to the temperatures. Since for higher temperatures the oil viscosity decreases, Fig.(2,b), while the oil velocity at the top of the pipe increases, Fig.(8,a) and Fig.(14,a), it seems that the height of the dune is adjusted in order to have roughly the same friction for every temperature. This hypothesis needs further investigation.

Another important information lost in the 1D analysis is the vertical distribution of the different variables. What can be seen from Fig.(8,a) and Fig.(14,a) is that the axial velocity profile is not flat but has a rather parabolic shape, because of the low Reynolds number. If the debris field is stratified, the maximum velocity is found at the top of the pipe, where the lighter fluid is. If the debris field is dispersed, the velocity profile is more symmetric.

This is due to the fact that the shape of the velocity profile is determined by the mixture viscosity, which depends on the wax volume fraction.

The non-uniform axial velocity field is the reason for the increase in time of the wax-in-oil slurry. If the velocity profile was flat, the wax chips could travel only as fast as the pig and accumulate in front of its body. However, because every viscous fluid respects the no-slip condition at the wall, the velocity at the center of the pipe must be higher than the mean velocity. In the case of a single-phase laminar motion, the maximum velocity is twice the mean one. The wax chips at the center of the pipe travel farther than the pig until they settle at a certain distance. Since the velocity at the boundary layer approaches zero, the fallen chips are slower than the pig, and after a certain period they will be re-scraped and re-injected into the pipe. The viscosity of the wax-in-oil slurry, shown in Fig.(8,a) and Fig.(14,a), influences the particle deposition. A high viscosity increases the friction, slowing down the chips, but reduces the settling, delaying the deposition.

As far as the pressure drop is concerned, the results in Fig.(6) and Fig.(12), show that it is mostly influenced by the temperature rather than the particle diameter. The purpose of Fig.(6) and Fig.(12) is to quantify the pressure drop increase due to the debris field. Despite the pressure drop being higher at lower temperatures, the debris field has a greater influence for higher temperatures. The pressure drop increases with time because of the increased suspended debris. This behavior must be carefully monitored to estimate the risk of a wax plug. As time goes by, the pump may not be able to deliver enough pressure, and the pig may slow down and stop. In the present model this scenario cannot take place because of the fixed flow rate boundary condition. This constraint allows the pressure to increase at will in order to satisfy the boundary condition.

Our results show that the temperature has a fundamental importance in determining the flow of the wax-in-oil slurry. In this work, the motion has been considered isothermal because a short and non-heated pipeline has been investigated. It would be necessary to introduce the energy equation to study heated or longer pipelines in the future.

Improved pig and slurry viscosity models are under investigation. Further experimental data are required to include the influence of non-Newtonian rheology and pour point. Nevertheless, the present formulation of debris-dependent viscosity is sufficient to show the qualitative mechanisms involved in debris transport and deposition. The effect of a bypass at the center of the pig is also under investigation.

6. Conclusions

A 3D numerical investigation of the fluid dynamics of the wax-in-oil slurry, subject to pigging operations, has been conducted in this work. The *drift flux* model has been used to simulate the flow of the slurry. The pig was modeled as a cylindrical body moving at constant speed in the pipe, due to the constant oil flow rate at the inlet. An injection boundary condition for the wax chips, equivalent to the scraping, but numerically more efficient, has been introduced. The properties of the two fluids have been experimentally derived. The influence of temperature and particle dimensions on the flow has been investigated.

The 3D simulations provide details, such as the axial velocity profiles, planar velocity vectors, and wax volume fraction field, which improve our comprehension of the dynamics of the process. This information can be used to improve the existing 1D models. Our group is currently investigating improvements of the present model as well as the influence of a bypass at the center of the pig.

7. Acknowledgments

The authors would like to thank the anonymous reviewers for their very helpful effort, their comments and suggestions improved the quality of the paper. The authors also thank Mr Rishabh Ishar for helpful suggestions in editing the manuscript. This research did not receive any specific grant from funding agencies in the public, commercial, or not-for-profit sectors.

References

Aarsnes, U. J. F., Ambrus, A., Di Meglio, F., Vajargah, A. K., Aamo, O. M., & van Oort, E. (2016). A simplified two-phase flow model using a quasi-equilibrium momentum balance. *International Journal of Multiphase Flow*, *83*, 77–85.

Aiyejina, A., Chakrabarti, D. P., Pilgrim, A., & Sastry, M. (2011). Wax formation in oil pipelines: A critical review. *International Journal of Multiphase Flow*, *37*, 671–694.

Al-Nassri, S. A., & Unny, T. (1981). Developing laminar flow in the inlet length of a smooth pipe. *Applied Scientific Research*, *36*, 313–332.

Asheim, H., & Grødal, E. (1998). Holdup propagation predicted by steady-state drift flux models. *International Journal of Multiphase Flow, 24*, 757–774.

Azevedo, L., Bracm, A., Nieckele, A., Naccxhe, M., Gomes, M. et al. (1996). Simple hydrodynamicmodels for the prediction of pig motions in pipelines. In *Offshore Technology Conference* (pp. 729–739). Offshore Technology Conference.

Azevedo, L., Braga, A., Nieckele, A., & Souza Mendes, P. (1999). simulating pipeline pigging operations. In *Proc. The Pipeline Pigging Conference, Stavanger, Norway* (pp. 1–21).

Barros Jr, J., Alves, D., Barroso, A., Souza, R., & Azevedo, L. (2005). Experimental validation of models for predicting wax removal forces in pigging operations. In *Proceedings of 18th International Congress of Mechanical Engineering, Ouro Preto, MG, Brazil* (pp. 6–11).

Barua, S. (1982). *An Experimental Verification and Modification of the McDonald-Baker Pigging Model for Horizontal Flow*. Ph.D. thesis University of Tulsa, OK.

Bhagwat, S. M., & Ghajar, A. J. (2014). A flow pattern independent drift flux model based void fraction correlation for a wide range of gas–liquid two phase flow. *International Journal of Multiphase Flow*, *59*, 186–205.

Braga, A., Azevedo, L., & Correa, K. (1999). Resistive force of wax deposits during pigging operations. *Journal of Energy Resources Technology*, *121*, 167–171.

Camenen, B. (2008). Settling velocity of sediments at high concentrations. *Proceedings in Marine Science*, *9*, 211–226.

Chen, S.-W., Liu, Y., Hibiki, T., Ishii, M., Yoshida, Y., Kinoshita, I., Murase, M., & Mishima, K. (2012). One-dimensional drift-flux model for two-phase flow in pool rod bundle systems. *International Journal of Multiphase Flow*, *40*, 166–177.

Clark, N., Van Egmond, J., & Nebiolo, E. (1990). The drift-flux model applied to bubble columns and low velocity flows. *International Journal of Multiphase Flow*, *16*, 261–279.

Deng, T., Gong, J., Zhou, J., Zhang, Y., & Li, H. (2014). Numerical simulation of the effects of vaporization on the motion of pig during pigging process. *Asia-Pacific Journal of Chemical Engineering*, *9*, 854–865.

Esmaeilzadeh, F., Mowla, D., & Asemani, M. (2009). Mathematical modeling and simulation of pigging operation in gas and liquid pipelines. *Journal of Petroleum Science and Engineering*, *69*, 100–106.

França, F., & Lahey, R. (1992). The use of drift-flux techniques for the analysis of horizontal two-phase flows. *International Journal of Multiphase Flow*, *18*, 787–801.

Galta, T. (2014). *Bypass Pigging of Subsea Pipelines Suffering Wax Deposition*. Master's thesis Institutt for petroleumsteknologi og anvendt geofysikk.

Gavrilyuk, S., & Fabre, J. (1996). Lagrangian coordinates for a drift-flux model of a gas-liquid mixture. *International Journal of Multiphase Flow*, *22*, 453–460.

Hosseinalipour, S., Khalili, A. Z., & Salimi, A. (2007a). Numerical simulation of pig motion through gas pipelines. In *16th Australian Fluid Mechanics Conference, Goald Coast Australia*. volume 12.

Hosseinalipour, S., Salimi, A., & Khalili, A. Z. (2007b). Transient flow and pigging operation in gas-liquid two phase pipelines. In *16th Australasian Fluid Mechanics Conference Crown Plaza, Gold Coast, Australia* (pp. 976–979).

Hovden, L., Labes-Carrier, C., Rydahl, A., Ronningsen, H., & Xu, Z. (2003). Pipeline wax deposition models and model for removal of wax by pigging: Comparison between model predictions and operational experience. In *Abstracts of Papers of the American Chemical Society* (pp. U936–U936). Amer Chemical Soc 1155 16TH ST, NW, Washington, DC 20036 USA volume 225.

Hu, Z., & Appleton, E. (2005). Dynamic characteristics of a novel self-drive pipeline pig. *Robotics, IEEE Transactions on*, *21*, 781–789.

Huang, Q., Wang, W., Li, W., Ren, Y., Zhu, F. et al. (2016). A pigging model for wax removal in pipes. In *SPE Annual Technical Conference and Exhibition* (pp. 1–11). Society of Petroleum Engineers.

Kim, D. K., Cho, S. H., Park, S. S., Rho, Y. W., Yoo, H. R., Nguyen, T. T., & Kim, S. B. (2003). Verification of the theoretical model for analyzing dynamic behavior of the pig from actual pigging. *KSME International Journal*, *17*, 1349–1357.

Kohda, K., Suzukawa, Y., & Furukawa, H. (1988). New method for analyzing transient flow after pigging scores well. *Oil and Gas Journal*, *86*, 40–47.

Lesani, M., Rafeeyan, M., & Sohankar, A. (2012). Dynamic analysis of small pig through two and three-dimensional liquid pipeline. *Journal of Applied Fluid Mechanics*, *5*, 75–83.

Lima, P., Alves, S. et al. (1995). Application of low density foam pigs offshore brazil. In *Annual Offshore Technology Conference* (pp. 529–529). Offshore Technology Conference volume 3.

Lima, P., Yeung, H. et al. (1998). Modeling of transient two-phase flow operations and offshore pigging. In *SPE Annual Technical Conference and Exhibition*. Society of Petroleum Engineers.

Lima, P., Yeung, H. et al. (1999). Modeling of pigging operations. In *SPE Annual Technical Conference and Exhibition*. Society of Petroleum Engineers.

Low Flow Study Project Team (2011). *Low Flow Impact Study FINAL REPORT*. Technical Report Alyeska Pipeline.

McDonald, A. E., & Baker, O. (1964). A method of calculating multiphase flow in pipe lines using rubber spheres to control liquid holdup. *Drilling and Production Practice*, (pp. 56–68).

Minami, K., & Shoham, O. (1995). Pigging dynamics in two-phase flow pipelines: Experiment and modeling. *Society of Petroleum Engineers*, *10*, 225–232.

Mirshamsi, M., & Rafeeyan, M. (2015). Dynamic analysis of pig through two and three dimensional gas pipeline. *Journal of Applied Fluid Mechanics*, *8*, 43–54.

Nguyen, T. T., Kim, D. K., Rho, Y. W., & Kim, S. B. (2001a). Dynamic modeling and its analysis for pig flow through curved section in natural gas pipeline. In *Computational Intelligence in Robotics and Automation, 2001. Proceedings 2001 IEEE International Symposium on* (pp. 492–497). IEEE.

Nguyen, T. T., Kim, S. B., Yoo, H. R., & Rho, Y. W. (2001b). Modeling and simulation for pig flow control in natural gas pipeline. *KSME International Journal*, *15*, 1165–1173.

Nguyen, T. T., Kim, S. B., Yoo, H. R., & Rho, Y. W. (2001c). Modeling and simulation for pig with bypass flow control in natural gas pipeline. *KSME International Journal*, *15*, 1302–1310.

Nguyen, T. T., Yoo, H. R., Rho, Y. W., & Kim, S. B. (2001d). Speed control of pig using bypass flow in natural gas pipeline. In *Industrial Electronics, 2001. Proceedings. ISIE 2001. IEEE International Symposium on* (pp. 863–868). IEEE volume 2.

Nieckele, A., Braga, A., & Azevedo, L. (2001). Transient pig motion through gas and liquid pipelines. *Journal of Energy Resources Technology*, *123*, 260–269.

Patrachari, A. R., & Johannes, A. H. (2012). A conceptual framework to model interfacial contamination in multiproduct petroleum pipelines. *International Journal of Heat and Mass Transfer*, *55*, 4613–4620.

Rusche, H. (2003). *Computational Fluid Dynamics of Dispersed Two-Phase Flows at High Phase Fractions*. Ph.D. thesis Imperial College London (University of London).

Saeidbakhsh, M., Rafeeyan, M., & Ziaei-Rad, S. (2009). Dynamic analysis of small pigs in space pipelines. *Oil & Gas Science and Technology-Revue de l'IFP*, *64*, 155–164.

Southgate, J. (2004). *Wax Removal Using Pipeline Pigs*. Ph.D. thesis Durham University.

Tan, G.-B., Liu, S.-H., Wang, D.-G., & Zhang, S.-W. (2015a). Spatio-temporal structure in wax–oil gel scraping at a soft tribological contact. *Tribology International*, *88*, 236–251.

Tan, G.-B., Liu, S.-H., Wang, D.-G., & Zhang, S.-W. (2015b). Tribological behaviours of wax-in-oil gel deposition in orthogonal cleaning process. *Tribology Letters*, *57*, 1–18.

Tan, G.-B., Wang, D.-G., Liu, S.-H., & Zhang, S.-W. (2014). Probing tribological properties of waxy oil in pipeline pigging with fluorescence technique. *Tribology International*, *71*, 26–37.

Tolmasquim, S. T., & Nieckele, A. O. (2008). Design and control of pig operations through pipelines. *Journal of Petroleum Science and Engineering*, *62*, 102–110.

Varadarajan, P. A., & Hammond, P. S. (2015). Numerical scheme for accurately capturing gas migration described by 1d multiphase drift flux model. *International Journal of Multiphase Flow*, *73*, 57–70.

Vorobev, A., & Boghi, A. (2016). Phase-field modelling of a miscible system in spinning droplet tensiometer. *Journal of Colloid and Interface Science*, *482*, 193–204.

Wang, Q., Sarica, C., & Chen, T. X. (2005). An experimental study on mechanics of wax removal in pipeline. *Journal of Energy Resources Technology*, *127*, 302–309.

Wang, Q., Sarica, C., & Volk, M. (2008). An experimental study on wax removal in pipes with oil flow. *Journal of Energy Resources Technology*, *130*, 043001.

Wang, W., & Huang, Q. (2014). Prediction for wax deposition in oil pipelines validated by field pigging. *Journal of the Energy Institute*, *87*, 196–207.

Wang, W., Huang, Q., Liu, Y., Sepehrnoori, K. et al. (2015). Experimental study on mechanisms of wax removal during pipeline pigging. In *SPE Annual Technical Conference and Exhibition* (pp. 1–25). Society of Petroleum Engineers.

Xu, X.-X., & Gong, J. (2005). Pigging simulation for horizontal gas-condensate pipelines with low-liquid loading. *Journal of Petroleum Science and Engineering*, *48*, 272–280.

An inertial two-phase model of wax transport in a pipeline during pigging operations

Boghi, Andrea

2017-04-15

Boghi A, Brown L, Sawko R, Thompson CP. (2017) An inertial two-phase model of wax transport in a pipeline during pigging operations. International Journal of Multiphase Flow, Volume 94, September 2017, pp. 17-30

https://doi.org/10.1016/j.ijmultiphaseflow.2017.04.007